CALCULATION OF THE RATE OF AMALGAM DECOMPOSITION IN A HORIZONTAL DECOMPOSER

Václav CEZNER, Petr NOVÁK, Ivo ROUŠAR and Vladimír MEJTA

Department of Inorganic Technology,
Prague Institute of Chemical Technology, 166 28 Prague 6

Received March 31st, 1982

The decomposition rate of the sodium or potassium amalgam in a horizontal decomposer was calculated with regard to three different forms of the amalgam surface, namely a horizontal plane, a half-spherical, and a half-ellipsoidal form. A comparison of the three models showed that the dependence of the amalgam decomposition rate on the driving force of the decomposition is in all cases analogous. In the region of low decomposition rates, all three models lead to practically the same decomposition rates.

One of the principal reactions in the electrolysis of brine by the amalgam method is the decomposition of the amalgam. This is carried out in the industrial practice mostly in horizontal decomposers, where the decomposition rate of the amalgam was calculated by Hostomský[1] on the assumption that the amalgam surface is planar. Similar calculations were done by Cezner[2], who assumed a cyllindrical form of the amalgam surface. In the present work, we assume that the cross section of the amalgam surface has the form of an ellipse, and the calculated reaction rates are compared with the previous models.

DESCRIPTION OF THE MODEL

We shall consider a horizontal amalgam decomposer When the amalgam flows through the decomposer, its concentration decreases and the rate of its decomposition changes accordingly. In a small section of the decomposer, the concentrations of the amalgam and alkali hydroxide and the temperature can be considered constant, otherwise they depend on the distance from the inlet.

A schematic cross section of model decomposer is shown in Fig. 1. The amalgam flows through a rectangular channel formed by graphite electrodes. The amalgam surface has a convex form of maximum height h_A. The alkali hydroxide solution above the amalgam has a level height y_K. The system is symmetrical with respect to a plane passing through the center of the channel, hence it is sufficient to consider only one half of the channel width, x_K, in the mathematical description. The origin of coordinates is placed on the electrolyte level in the center of the channel (Fig. 1).

Thus, the cathode surface is defined by $x = x_K$ and the anode contacts the cathode in the point (x_K, y_K). With respect to the calculations below, it is preferable to set the thickness l_a of the decomposition element (in the direction of the z axis) equal to y_K.

Assumptions Involved in the Theory

1) The system is in a stationary state. *2*) The heterogeneous system (gas bubbles in the electrolyte) can be treated as a continuum involving time-averages of the physical quantities. *3*) The potential gradient in the direction of the z axis is negligible against the x and y components. *4*) Temperature, pressure, and composition of the amalgam and electrolyte in the element is constant. *5*) The volume fraction of gas bubbles is in the whole element constant, hence a constant resistivity of the gas emulsion can be used. *6*) The anodic overvoltage in the decomposition element is due only to different activities of the alkali metal in the bulk of the amalgam ($a_{K,am}$) and at the interface ($a_{K,s}$), the latter quantity being on the whole amalgam surface the same. *7*) The voltage drop due to the current passing through the graphite and amalgam is negligible and the contact resistance between amalgam and graphite is also negligible. *8*) Spontaneous decomposition of the amalgam is negligible against its electrochemical decomposition. *9*) Inclination of the decomposer with respect to the z axis is negligible.

Basic Equations

The quantity of the alkali metal in the amalgam, which dissolves in the decomposition element, can be expressed according to the law of Faraday by the current

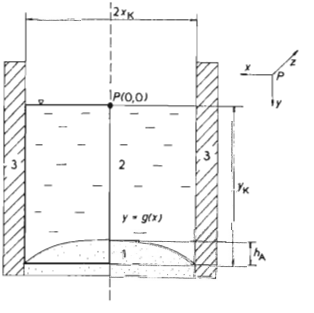

FIG. 1

Cross section of a horizontal model decomposer. x, y, z axes of coordinates, x_K, y_K dimensions of the decomposer elements, h_A height of amalgam meniscus, $g(x)$ profile of the anode surface, 1 amalgam anode, 2 alkali hydroxide solution, 3 graphite cathode

I_R flowing from the electrolyte into the graphite

$$I_R = l_a \int_0^{y_K} j_K \, dy \quad \text{for} \quad x = x_K \,. \tag{1}$$

Here, j_K denotes the normal component of the current density on the graphite surface, which can be calculated from the potential distribution in the decomposition element. This can in turn be calculated from the law of Ohm in the differential form and the current balance

$$j = -(1/\varrho_M) \operatorname{grad} \varphi \,, \quad \operatorname{div} j = 0 \,, \tag{2),(3}$$

where j is the vector of current density and ϱ_M the resistivity of the gas emulsion. The electric potential φ of the electrolyte is referred to the equilibrium potential of the hydrogen electrode in the same solution. Accordingly, the potential in the liquid at the graphite surface is equal to the negative value of the hydrogen overvoltage on graphite, $-\eta_K$, at the current density j_K. The potential in the bulk of the electrolyte is then equal to the sum of the absolute value of the hydrogen overvoltage and the ohmic voltage drop in the electrolyte along a current line joining the considered point with the graphite surface (Fig. 2). The value of $\varphi_{A,s}$ on the surface of the amalgam anode is equal to the electromotive force of the cell diminished by the anodic overvoltage. The value of $\varphi_{A\text{-}am}$ in the amalgam is equal to zero, owing to our assumption 7).

The electric potential in the electrolyte in a function of coordinates defined by the Laplace equation

$$\nabla^2 \varphi = 0 \,, \tag{4}$$

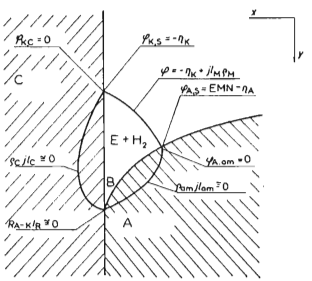

FIG. 2

Distribution of the electric potential along a current line. φ potential, EMN electromotive force of the cell, j current density along the current line of length l, ϱ resistivity, I_R total decomposition current in the element, R_{A-K} electric resistance in point B of the anode–cathode contact. Subscripts denote: A anode, K cathode, s electrolyte side of the electrode surface, M bubble-eletrolyte mixture, am amalgam, C graphite

which follows from Eqs (*2*) and (*3*). By assumption *3*), Eq. (*4*) gives

$$\partial^2\varphi/\partial x^2 + \partial^2\varphi/\partial y^2 = 0\,. \tag{5}$$

The boundary conditions are derived as follows:

1) The cathodic current density is given as a function of the overvoltage for hydrogen evolution[3,4]

$$j_K = j_0\{\exp\left[(\eta_K(\boldsymbol{F}/\boldsymbol{RT} - 1/b_c)\right] - \exp\left(-\eta_K/b_c\right)\}\,, \tag{6}$$

where j_0 denotes apparent exchange current density and

$$b_c = b/\ln 10 = \boldsymbol{RT}/\alpha\boldsymbol{F}\,. \tag{7}$$

If $|\eta_K| \gg \boldsymbol{RT}/\boldsymbol{F}$ (*i.e.*, at higher current densities), Eq. (*6*) can be simplified to the Tafel equation

$$\eta_K = a - b\log|j_K|\,. \tag{8}$$

Here, the current density j_K must be determined from Eq. (*2*). Since the potential at the cathode surface is equal to $-\eta_K$, we arrive at the boundary condition on the cathode surface for $x = x_K$:

$$(-\partial\varphi/\partial x)_{K,s} = j_0\varrho_M\{\exp\left[-\varphi_{K,s}(\boldsymbol{F}/\boldsymbol{RT} - 1/b_c)\right] - \exp\left(\varphi_{K,s}/b_c\right)\} \tag{9}$$

or for large overvoltage

$$-(\partial\varphi/\partial x)_{K,s} = \varrho_M\exp\left[(\varphi_{K,s} + a)/b_c\right], \quad x = x_K\,. \tag{10}$$

2) If the activity of the alkali metal is constant at the whole amalgam-electrolyte interface and the contact resistance between the amalgam and graphite is negligible, then the potential at the amalgam surface is equal to the difference between the electromotive force, E_{am}, of the amalgam–hydrogen cell at the given conditions, and the anodic overvoltage. With respect to the assumption *6*), the anode potential representing the boundary conditions can be expressed as

$$\varphi_{A,s} = E_{am} - (\boldsymbol{RT}/\boldsymbol{F})\ln\left(a_{K,am}/a_{K,s}\right), \quad y = g(x)\,, \tag{11}$$

where the function $g(x)$ describes the form of the anode surface.

3) Since the current does not pass across the other boundaries of the considered element, we have

$$\partial\varphi/\partial y = 0\,, \quad y = 0\,; \quad \partial\varphi/\partial x = 0\,, \quad x = 0\,. \tag{12),(13}$$

The shape of the amalgam surface is approximated by one half of an ellipse

$$y = g(x) = y_K - h_A \sqrt{[1 - (x/x_K)^2]}, \quad x \in \langle 0, x_K \rangle, \tag{14}$$

where h_A denotes the maximum height of the amalgam surface in the middle of the channel.

Rearrangement of the Basic Equations to a Dimensionless Form

For the numerical solution, dimensionless parameters are preferred. A characteristic dimension is the height of the electrolyte level, y_K (Fig. 1). The dimensionless coordinates are

$$X = x/y_K, \quad Y = y/y_K. \tag{15), (16}$$

The dimensions of the model are transformed in a similar way

$$X_K = x_K/y_K, \quad Y_K = 1, \tag{17), (18}$$

$$G(X) = 1 - (h_A/y_K) \sqrt{[1 - (X/X_K)^2]}. \tag{19}$$

The dimensionless thickness of the element is also equal to 1.

The characteristic voltage can be set equal to $-b_e$ (Eq. (7)). The dimensionless potential E^* is then defined as

$$E^* = \frac{a + \varphi}{b_e} + \ln \frac{\varrho_M y_K}{b_e}. \tag{20}$$

It is obvious that E^* becomes equal to zero if

$$\varphi_0 = -a + b_e \ln (b_e/\varrho_M y_K). \tag{21}$$

On introducing Eqs (15), (16), and (20) into the Laplace equation (5), we obtain an equation of the same form

$$\partial^2 E^*/\partial X^2 + \partial^2 E^*/\partial Y^2 = 0. \tag{22}$$

Similarly,

$$\partial E^*/\partial X = 0, \quad X = 0; \quad \partial E^*/\partial Y = 0, \quad Y = 0. \tag{23), (24}$$

On introducing Eqs (15)–(20) into the boundary condition (9) and assuming that $\alpha_K \approx 0{\cdot}5$, we obtain after rearrangement

$$-(\partial E^*/\partial X) = \exp(E^*) - \exp(-E^* + Z_K), \quad X = X_K, \tag{25}$$

where

$$Z_K = 2 \ln (j_0 \varrho_M y_K / b_c) . \tag{26}$$

Similarly, it follows from the Tafel equation (*10*) that

$$-(\partial E^* / \partial X) = \exp (E^*) , \quad X = X_K . \tag{27}$$

In further calculations, only Eq. (*25*) will be used as the boundary condition for the cathode, since it is valid for any value of the current density, whereas Eq. (*27*) applies only to high current densities. Both Eqs (*27*) and (*10*) lead to infinite negative potential for zero current density, which would cause serious troubles in the numerical iteration procedure. In Eq. (*25*), zero current density corresponds to the dimensionless potential $Z_K/2$; *i.e.*, the boundary condition is finite in the whole region of current densities.

The boundary condition for the anode involves all physical quantities characterizing the given system

$$E^* = \frac{a + \varphi_{A,s}}{b_c} + \ln \frac{\varrho_M y_K}{b_c} . \quad Y = G(X) . \tag{28}$$

The potential $\varphi_{A,s}$ is given by Eq. (*11*). The right-hand side of Eq. (*28*) is constant for the whole anode surface; we shall call it the dimensionless cell voltage and denote it as Z_R. With regard to Eq. (*26*) we obtain from Eq. (*28*)

$$Z_R = \varphi_{A,s}/b_c + \tfrac{1}{2} Z_K . \tag{29}$$

The negative value of the gradient of the dimensionless potential E^* will be called the dimensionless current density. The maximum current density flows in the place where the anode contacts the cathode ($X = X_K$, $Y = 1$). In the dimensionless coordinates, the cathode surface area is according to our model equal to 1. Thus, dimensionless decomposition current J_R is identical with the mean value of the dimensionless cathodic current density and can be calculated as

$$J_R = - \int_0^1 (\partial E^* / \partial X) \, \mathrm{d}Y \quad \text{for} \quad X = X_K . \tag{30}$$

The relation between J_R and the decomposition current I_R flowing through the element follows from Eqs (*1*) and (*30*) combined with (*2*), (*15*)–(*18*)

$$J_R = I_R \varrho_M / b_c l_a . \tag{31}$$

Solution of Laplace's Equation for the Model System

The problem defined by Eqs (*22*)–(*28*) will be solved with respect to the complicated boundary of the model in the following way. By a suitable transformation of the variables, the ellipse forming the anode surface will be transformed to a straight line parallel to the X axis. The transformed equations will then be solved by the finite-difference method with unequal grid spacing.

In general, if the boundary of the system is given by the function $G = G(\xi)$ it can most simply be transformed to a rectangular region by introducing the variables

$$\xi = X\,, \quad \eta = Y/G(\xi)\,. \qquad (32), (33)$$

In our case, the function $G(\xi)$ is given by Eq. (*19*). Accordingly, the Laplace's equation (*22*) is transformed to

$$\frac{\partial^2 E^*}{\partial \xi^2} - \frac{\partial^2 E^*}{\partial \xi \partial \eta}\,\frac{2G'\eta}{G} + \frac{\partial^2 E^*}{\partial \eta^2}\,\frac{1 + \eta^2 G'^2}{G^2} - \frac{\partial E^*}{\partial \eta}\,\frac{GG'' - 2G'^2}{G^2}\,\eta = 0\,. \qquad (34)$$

The boundary conditions are obtained by transformation of Eqs (*23*), (*24*), (*28*), and (*25*):

$$\frac{\partial E^*}{\partial \xi} = 0\,, \quad \xi = 0\,; \quad \frac{\partial E^*}{\partial \eta} = 0\,, \quad \eta = 0\,; \qquad (35), (36)$$

$$E^* = Z_R\,. \quad \eta = 1\,; \qquad (37)$$

$$-\frac{\partial E^*}{\partial \xi} + \frac{\partial E^*}{\partial \eta}\,\eta\,\frac{G'}{G} = \exp(E^*) - \exp(-E^* + Z_K)\,, \quad \xi = \xi_K\,. \qquad (38)$$

The dimensionless anodic current density is given by the negative potential derivative with respect to the normal, N, to the curve G.

$$-\frac{\partial E^*}{\partial N} = -\frac{1}{\sqrt{(1 + G'^2)}}\left(\frac{\partial E^*}{\partial \eta}\,\frac{1 + \eta G'^2}{G} - \frac{\partial E^*}{\partial \xi}\,G'\right), \quad \eta = 1\,. \qquad (39)$$

Since the potential at the anode is constant (Eq. (*35*)), Eq. (*39*) is simplified to

$$-\frac{\partial E^*}{\partial N} = -\frac{\partial E^*}{\partial \eta}\,\frac{\sqrt{(1 + G'^2)}}{G}\,, \quad \eta = 1\,. \qquad (40)$$

The dimensionless decomposition current, J_R, is given by the integral of the normal current densities along the length of the cathode

$$J_R = -\int_0^1 \left(\frac{\partial E^*}{\partial \xi} - \frac{\partial E^*}{\partial \eta} \eta \frac{G'}{G} \right) d\eta , \quad \xi = \xi_K . \tag{41}$$

It can also be calculated by combining this equation with Eq. (38)

$$J_R = \int_0^1 [\exp(E^*) - \exp(-E^* + Z_K)] \, d\eta , \quad \xi = \xi_K . \tag{42}$$

In the above equations, primes denote differentiation with respect to ξ.

The potential distribution can be calculated by the finite-diference method[5]. The continuous space of the variables ξ and η is replaced by a two-dimensional, rectangular network. The problem, then, consists in finding a function given by approximate numerical values in the grid points and obeying the partial differential equation (34) with the boundary conditions (35)–(38). By replacing the derivatives with linear combinations of the function values in the grid points, Eq. (34) gives rise to a system of mn linear equations whose solution is the sought function (m and n denote the numbers of grid points in the directions of the ξ and η axes).

Since the dimensionless voltage Z_R can practically attain values from 1 to 19 and the dimensionless current density can at the point of contact of the anode with the cathode ($\xi = \xi_K$, $\eta = 1$) attain the order of 10^8 (for the highest Z_R value), decreasing as much as by five orders of magnitude with decreasing η, the grid intervals must be chosen so as to describe these changes with a sufficient accuracy. Therefore, a grid with unequal spacing must be used, where with increasing coordinates the grid interval decreases by a geometric series with a quotient q_h (Fig. 3).

To approximate the derivatives, the following equations (43)–(45) were used for points inside the field and (46) for the boundaries.

$$\left(\frac{\partial E^*}{\partial \xi} \right)_{i,j} \approx \frac{E^*_{i+1,j} h_{i-1}^2 + E^*_{i,j}(h_i^2 - h_{i-1}^2) - E^*_{i-1,j} h_i^2}{h_i h_{i-1}(h_i + h_{i-1})} \tag{43}$$

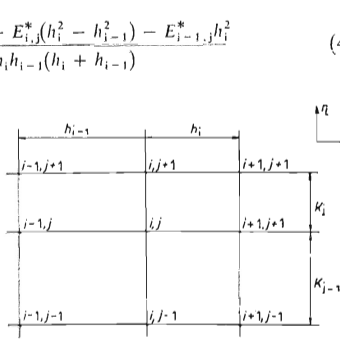

FIG. 3
Scheme of nonuniform coordinate grid

$$\left(\frac{\partial^2 E^*}{\partial \xi^2}\right)_{i,j} \approx \frac{E^*_{i+1,j} h_{i-1} - E^*_{i,j}(h_i + h_{i-1}) + E^*_{i-1,j} h_i}{0{\cdot}5 h_i h_{i-1}(h_i + h_{i-1})} \tag{44}$$

$$\left(\frac{\partial^2 E^*}{\partial \xi\, \partial \eta}\right)_{i,j} \approx \{[E^*_{i+1,j+1} h^2_{i-1} + E^*_{i,j+1}(h_i^2 - h^2_{i-1}) - E^*_{i-1,j+1} h_i^2]\, k^2_{j-1} +$$
$$+ [E^*_{i+1,j} h^2_{i-1}(h_i^2 - h_{i-1}^2) - E^*_{i-1,j} h_i^2]\,(k_j^2 - k^2_{j-1}) -$$
$$- [E^*_{i+1,j-1} h^2_{i-1} + E^*_{i,j-1}(h_i^2 - h^2_{i-1}) - E^*_{i-1,j-1} h_i^2]\, k_j^2\}/$$
$$/[h_i h_{i-1} k_j k_{j-1}(h_i + h_{i-1})(k_j + k_{j-1})] \tag{45}$$

$$\left(\frac{\partial E^*}{\partial \eta}\right)_{i,n} \approx \frac{E^*_{i,n}(h^2_{n-2} + 2h_{n-1}h_{n-2}) - E^*_{i,n-1}(h_{n-1} + h_{n-2})^2 + E^*_{i,n-2} h^2_{n-1}}{h_{n-1} h_{n-2}(h_{n-1} + h_{n-2})} \tag{46}$$

It is preferable to express the derivatives of the function G numerically, since in the potential derivatives the curve sections are also approximated by secants and the errors of the method are thus partially compensated. In the point $i = m$ (where the anode contacts the cathode), the function G has different derivatives from the left and from the right.

For the sake of simplification, it was assumed that the function G attains the value of 1 already in the point $i = m - 1$. The boundary of the system was replaced by a parabola passing through the points $m - 2$, $m - 1$, and m on the anode surface (Fig. 4). The first and second derivatives of G in the point $i = m$ are equal to zero and in the point $i = m - 1$ are calculated from Eqs (*43*) and (*44*). In the limiting case, where $h_{m-1} \to 0$, the solution of the partial differential equation for the modified function G becomes equal to that for the original one. The ratio of the grid interval h_{m-1} to the anode height h_A was chosen in the range from 1 : 48 to 1 : 108 000 increasing with the value of Z_R, since the portion of the total current flowing near the point of contact of the electrodes increased also. The correctness of the results was checked by decreasing the

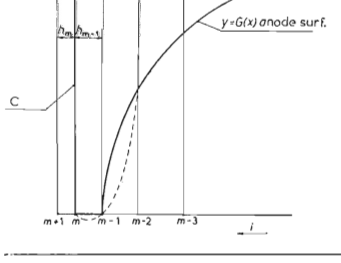

FIG. 4

Function G describing the form of the anode surface in a model system at the anode--cathode contact

value of h_{m-1} by the factor of 1/2; the resulting change of the decomposition current was less than 1%.

To simplify the calculation program, the system of grid points was supplemented with fictitious grid points beyond each boundary. Thus, the potential values on the boundaries could be calculated from formally the same equations as inside the field (in the electrolyte). The values of the fictitious potentials in the added grid points were determined from the boundary conditions.

The system of linear equations obtained from Eq. (*34*) by using the difference formulas for the derivatives can be written as

$$-\left(E^*_{i+1,j+1}h^2_{i-1}h^2_{j-1} - E^*_{i-1,j+1}h^2_i k^2_{j-1} - E^*_{i+1,j-1}h^2_{i-1}k^2_j + \right.$$
$$\left. + E^*_{i-1,j-1}h^2_i k^2_j\right) G_{2,i}/H_i + E^*_{i+1,j}\left[2h_{i-1}K_j - h^2_{i-1}G_{2,i}(k^2_j - k^2_{j-1})\right]/H_i +$$
$$+ E^*_{i-1,j}\left[2h_i K_j + h^2_i G_{2,i}(k^2_j - k^2_{j-1})\right]/H_i + E^*_{i,j+1}\left[2k_{j-1}G_{1,i} - \right.$$
$$\left. - k^2_{j-1}(h^2_i - h^2_{i-1})\, G_{2,i}/H_i - k^2_{j-1}G_{3,i}\right] + E^*_{i,j-1}\left[2k_j G_{1,i} + k^2_j(h^2_i - \right.$$
$$\left. - h^2_{i-1})\, G_{2,i}/H_i + k^2_j G_{3,i}\right] - E^*_{i,j}\left[2(h_i + h_{i-1})\, K_j/H_i + 2(k_j + k_{j-1})\, G_{1,i} + \right.$$
$$\left. + (h^2_i - h^2_{i-1})\,(k^2_j - k^2_{j-1})\, G_{2,i}/H_i + (k^2_j - k^2_{j-1})\, G_{3,i}\right] = 0\,, \qquad (47)$$

where $i \in \langle 1, m\rangle$, $j \in \langle 1, n-1\rangle$, and

$$G_{1,i} = (1 + \eta^2_j G'^2_i)/G^2_i\,, \qquad (48)$$

$$G_{2,i} = 2\eta_j G'_i/G_i\,, \qquad (49)$$

$$G_{3,i} = (G_i G''_i - 2G'^2_i)\,\eta_j/G^2_i\,, \qquad (50)$$

$$\eta_j = \sum_{i=0}^{j-1} k_i\,, \quad H_i = h_i h_{i-1}(h_i + h_{i-1})\,, \qquad (51).(52)$$

$$K_j = k_j k_{-1}(k_j + k_{j-1})\,. \qquad (53)$$

Equation (*47*) is not suitable for the anode surface, since in this case Eq. (*37*) gives

$$E^*_{i,n} = Z_R\,, \quad i \in \langle 1, m\rangle\,. \qquad (54)$$

An equation for the fictitious potentials in the outer grid points is obtained from Eqs (*35*), (*36*), (*38*), and (*43*). If no current flows through the boundary, then

$$E^*_{i-1,j} = \frac{E^*_{i+1,j}h^2_{i-1} + E^*_{i,j}(h^2_i - h^2_{i-1})}{h^2_i}\,, \qquad (55)$$

where $i = 1$, $j \in \langle 1, n\rangle$; and further

$$E^*_{i,j-1} = \frac{E^*_{i,j+1}k^2_{j-1} + E^*_{i,j}(k^2_j - k^2_{j-1})}{k^2_j}\,, \qquad (56)$$

where $j = 1$, $i \in \langle 1, m\rangle$.

The solution of the elliptic partial differential equation in the given space region converges if the boundary conditions are given as constant values of the variable (in our case E^*) on the boundaries. If the boundary values change in the course of the iterations, they should change only little in comparison with the changes of the variable (E^*) inside the region. To fulfil this requirement, the value of E^* outside the cathode ($E^*_{m+1,j}$) was corrected during every iteration by using a formula derived from Eq. (*38*)

$$E^{*(\tau)}_{i+1,j} = E^{*(\tau-1)}_{i+1,j}(1 - \psi) + \psi\{-[\exp(E^{*(\tau-1)}_{i,j}) - \exp(-E^{*(\tau-1)}_{i,j} + Z_K)] \times$$
$$\times H_i/h^2_{i-1} - E^{*(\tau-1)}_{i,j}(h^2_i - h^2_{i-1})/h^2_{i-1} + E^{*(\tau-1)}_{i-1,j}h^2_i/h^2_{i-1}\}, \qquad (57)$$

where $i = m$, $j \in \langle 1, n\rangle$, τ denotes the order number of the iteration, and the coefficient ψ was optimized by trial and error as $\psi \leqq 0{\cdot}2$.

The system of $m(n-1)$ linear equations (*47*) for the same number of unknowns (from hundreds to thousands) was solved by a modified iterative overrelaxation method[4,5]. If the estimated values of $E^*_{i,j}$ are introduced into Eq. (*47*), its right-hand side is different from zero and is called the residuum, $R_{i,j}$. Eq. (*47*) can be converted to a system of equations of the type

$$E^{*(\tau+1)}_{i,j} = E^{*(\tau)}_{i,j} + \omega_{i,j}R^{(\tau)}_{i,j}, \quad i \in \langle 1, m\rangle, \quad j \in \langle 1, n-1\rangle, \qquad (58)$$

where $E^{*(\tau+1)}_{i,j}$, $E^{*(\tau)}_{i,j}$ denote approximate potential values in the grid point (i, j) in the corresponding iterations and $\omega_{i,j}$ is the overrelaxation factor. The system of equations (*58*) converges to the solution vector of Eqs (*47*) if the factor $\omega_{i,j}$ is properly chosen. We used the formula

$$\omega_{i,j} = \omega_0/[2|(h_i + h_{i-1})K_j/H_i| + 2|(k_j + k_{j-1})G_{1,i}| +$$
$$+ |(h^2_i - h^2_{i-1})(k^2_j - k^2_{j-1})G_{2i}/H_i| + |(k^2_j - k^2_{j-1})G_{3,i}|] \qquad (59)$$

for $i \in \langle 1, m\rangle$ and $j \in \langle 1, n-1\rangle$.

On the right-hand side there is a ratio of the constant ω_0 and the modified coefficient at the term $E^*_{i,j}$ in Eq. (*47*). The constant ω_0 lies in the interval $\langle 1, 2\rangle$ and controls the rate of convergence of the iteration process. It depends on the matrix dimension and must be determined empirically by evaluating the rate of convergence of several calculations with a relatively small number of iterations.

After solving the system of equations (*58*), the potential values on the cathode surface in the grid points $i = m$, $1 \leqq j \leqq n$, are known and can be used to calculate the dimensionless current flowing through the decomposition element. The integral in Eq. (*42*) can with an accuracy corresponding to the method used be replaced with the sum

$$J_{R,K} = \tfrac{1}{2}\sum_{j=1}^{n-1}[\exp(E^*_{m,j}) + \exp(E^*_{m,j+1}) - \exp(-E^*_{m,j} + Z_K) -$$
$$- \exp(-E^*_{m,j+1} + Z_K)]\,k_j. \qquad (60)$$

To judge the correctness of the calculations, we calculated also the anodic current by numerical integration over the anode surface from Eq. (*40*) combined with (*43*)

$$J_{R,A} = -\sum_{i=1}^{m-1} \left[(E^*_{i,n}\sqrt{G_{1,i}} + E^*_{i+1,n}\sqrt{G_{1,i+1}})\,(h^2_{n-2} + 2h_{n-1}h_{n-2}) - \right.$$
$$- (E^*_{i,n-1}\sqrt{G_{1,i}} + E^*_{i+1,n-1}\sqrt{G_{1,i+1}})\,(h_{n-1} + h_{n-2})^2 + (E^*_{i,n-2}\sqrt{G_{1,i}} +$$
$$\left. + E^*_{i+1,n-1}\sqrt{G_{1,i+1}})\,h^2_{n-1} \right] s_i/2H_{n-1}\,, \qquad (61)$$

where s_i denotes the length of the line connecting the neighbouring grid points on the anode surface, approximating the surface curve

$$s_i = \sqrt{[(G_i + G_{i+1})^2 + h^2_{i+1}]}\,. \qquad (62)$$

The magnitude of the step k_j, representing the mutual distance of the grid points on the cathode, must be chosen so that the current flowing through the section k_j be negligible against the total decomposition current for every term of the sum (*60*), especially the one corresponding to k_{n-1} (the contact between the anode and cathode). The steps k_j increase with decreasing j by a geometric series with a chosen quotient q_h lying between 1 and 1·4; for higher values of q_h the rate of convergence of the iteration solution of the equation system (*58*) decreases eventually to zero.

RESULTS OF CALCULATIONS

The calculations were carried out on an ICL 4-72 computer with a program elaborated in FORTRAN. The input data were: Dimensionless voltage of the decomposition element Z_R, parameter Z_K, dimensionless simplexes X_K and h_A/y_K. The calculation was stopped as soon as the value of the highest residuum decreased below $1 \cdot 10^{-4}$. The results are given in Table I together with the input data. The accuracy of the calculation is indicated by the agreement of the dimensionless decomposition current flowing through the cathode (Eq. (*60*)) with that flowing through the anode (Eq. (*61*)). The deviations are in the range from 0·9 to 8·7% depending on the number of grid points and on the number of iterations. They decrease slowly with increasing number of iterations; since the values of $J_{R,K}$ and $J_{R,A}$ approach the correct value from different sides, their arithmetic mean, J_R, can be considered as most correct.

The parameter Z_R characterizes the rate of the decomposition reaction at the corresponding current. It is a measure of the driving force of the process and involves the influence of the reactant concentration, overvoltage, and ohmic resistance. At low values of Z_R, corresponding to low amalgam concentration and low electromotive force, the decomposition rate depends on the electrode overvoltage. The resistance of the hydrogen emulsion is relatively low and the distribution of the current density

on both electrodes is uniform. Under these conditions, the process is influenced also by the dimensions of the system, parameter X_K, and partial anodic current on the cathode, involved in the parameter Z_K (Table I). At high values of Z_R, most of the decomposition current flows in the close vicinity of the anode-cathode contact. This means that the space between the electrodes is filled with gas and the resistance of the gas emulsion is much higher than that of the pure electrolyte. The influence of the parameters X_K and Z_K is negligible in this case.

To evaluate the influence of the form of the amalgam surface, the calculated decomposition currents were compared with the data referring to a planar amalgam level[1], *i.e.*,

$$G(X) = 1 , \quad X \in \langle 0, X_K \rangle . \tag{63}$$

The data given by Hostomský[1] are given in Table II in terms of our dimensionless variables.

As another case, we considered a horizontal decomposer in which the amalgam level close to the anode-cathode contact has the form of a quarter of a circle and

TABLE I

Calculated values of dimensionless decomposition current J_R in an amalgam decomposer. Elliptical approximation of the amalgam surface, $h_A/y_K = 0{\cdot}1$. Z_R dimensionless voltage of decomposition cell (Eq. (*29*)), Z_K parameter defined by Eq. (*26*), X_K dimensionless width of decomposition element, $J_{R,K}$ dimensionless cathodic current from Eq. (*60*), $J_{R,A}$ dimensionless anodic current from Eq. (*61*), q_h quotient of nonuniform coordinate grid, mn dimensions of the grid, t time of calculation (in s) on an ICL-4-72 computer

Z_R	Z_K	X_K	$J_{R,K}$	$J_{R\cdot A}$	J_R	q_h	mn	t
18·5595	0	0·26	1 990·8	2 092·8	2 042	1·4	36 × 39	1 440
15·2901	0	0·26	913·27	1 000·38	956·8	1·4	36 × 39	1 526
10·0000	0	0·26	96·343	105·283	100·81	1·3	33 × 35	1 602
4·7099	0	0·26	8·5001	8·8423	8·671	1·3	18 × 24	281
1·4405	0	0·26	1·2816	1·3283	1·305	1·3	15 × 21	198
4·7099	0	0·34	8·4592	8·9986	8·729	1·3	20 × 24	310
1·4405	0	0·34	1·3554	1·4244	1·390	1·3	17 × 21	227
4·7099	−10	0·26	8·5843	8·8943	8·739	1·3	18 × 24	270
1·4405	−10	0·26	1·5489	1·5626	1·556	1·3	15 × 21	198
4·7099	0	0·10	8·8566	9·1876	9·022	1·3	14 × 24	212
1·4405	0	0·10	1·0433	1·1228	1·083	1·3	12 × 21	148

otherwise it is plane (Fig. 5). Hence,

$$G(X) = 1 - \left[\left(\frac{h_A}{y_K}\right)^2 - \left(X - X_K + \frac{h_A}{y_K}\right)^2\right]^{1/2} \qquad (64)$$

for $X \in \langle X_K - h_A/y_K, X_K \rangle$, and

$$G(X) = 1 - \frac{h_A}{y_K} \quad \text{for} \quad X \in \left\langle 0, X_K - \frac{h_A}{y_K} \right\rangle . \qquad (65)$$

TABLE II

Dependence of dimensionless decomposition current J_R on the parameter Z_R according to Hostomský. Planar approximation of the amalgam surface

Z_R	J_R		
	$X_K = 0{\cdot}2$	$X_K = 0{\cdot}1$	$X_K = 0{\cdot}05$
−1·609	0·312	0·388	0·424
−0·916	0·497	0·576	0·609
−0·223	0·759	0·834	0·862
0·336	1·04	1·11	1·13
0·693	1·25	1·32	1·34
1·386	1·77	1·82	1·84
2·079	2·43	2·48	2·49
2·639	3·09	3·13	3·15
2·996	3·58	3·61	3·62
3·689	4·68	4·70	4·70
4·382	6·03	6·05	6·05
4·942	7·34	7·34	7·34
5·298	8·20	8·20	8·20
5·991		10·0	
6·685		12·2	
7·244		14·1	
7·601		15·5	
8·294		18·3	
8·987		21·4	
9·547		25·0	
9·903		25·8	
10·597		29·4	
11·290		33·2	
11·849		36·5	
12·206		38·6	
12·899		42·8	

On the amalgam surface, we have the boundary condition (*28*). The vicinity of the three-phase contact is modelled according to Fig. 4. The results of calculations are given in Table III.

It is seen from the comparison of the mentioned models that the planar model of the amalgam surface gives for $Z_R < 4$ significantly lower values of the decomposition rate than the other models. If the cross section of the surface is approximated by a circular arc and a straight line, the results are higher than in the case of an ellipse (Tables I and III). The form of the dependences is quite the same, since most of the

TABLE III

Calculated dimensionless decomposition current J_R in a horizontal amalgam decomposer. Approximation of the amalgam surface according to Fig. 5; $h_A/y_K = 0{\cdot}1$. See Table I for symbols

Z_R	Z_K	X_K	$J_{R,K}$	$J_{R,A}$	J_R	q_h	mn	t
18·5595	0	0·26	2 717·6	2 808·4	2 763	1·4	36 × 39	1 782
15·2901	0	0·26	1 303·9	1 400·7	1 352	1·4	36 × 39	1 759
10·0000	0	0·26	146·11	155·60	150·9	1·3	33 × 35	1 444
4·7099	0	0·26	10·281	10·844	10·56	1·3	18 × 24	353
1·4405	0	0·26	1·3549	1·5302	1·443	1·3	15 × 21	173
4·7099	0	0·34	10·616	10·910	10·76	1·3	19 × 24	230
1·4405	0	0·34	1·4444	1·5359	1·490	1·3	16 × 21	227
4·7099	−10	0·26	10·325	10·902	10·61	1·3	18 × 24	306
1·4405	−10	0·26	1·6165	1·8033	1·710	1·3	15 × 21	173

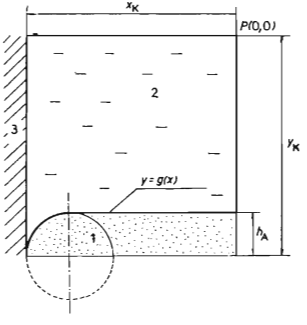

FIG. 5

Decomposition element in a horizontal decomposer. The amalgam surface approximated by a quarter-circle and a straight line. 1 anode, 2 electrolyte, 3 graphite cathode. See Fig. 1 for symbols

decomposition current flows near the contact point of both electrodes, where both models of the anode are very similar. The more distant regions of the anode surface are practically without influence on the decomposition rate. It follows from our results that the conditions in vertical and horizontal amalgam decomposers are nearly the same if the dimensionless parameters are the same.

CONCLUSIONS

The dependence of the decomposition rate of the amalgam on the driving force of the reaction is for all three models analogous. At low values of the driving force, all three models lead to practically the same values of the decomposition rate, whereas at higher values (high amalgam concentration, low hydrogen overvoltage) the planar model of the amalgam surface leads to much too low decomposition current. For a sufficiently wide channel, the model according to Fig. 5 is closest to reality (straight line with two arcs). The amalgam surface in rather narrow channels comes close to one half of an ellipse (Eq. (*14*)), and in very narrow ones to a half-circle. The most important part of the surface is close to the three-phase interface. The contact angle is probably smaller than the assumed value of 180°. For comparison with experiments and technical calculations, our models of the curved amalgam surface are therefore preferable, although the true values of the decomposition current may be somewhat lower than calculated.

LIST OF SYMBOLS

a, b	constants of the Tafel equation for hydrogen overvoltage on graphite (V)
a_K	activity of potassium in amalgam
b_e	constant defined by Eq. (*7*)
E^*	dimensionless potential defined by Eq. (*20*)
F	Faraday's constant (96 487 C/mol)
G	dimensionless function describing the amalgam surface
$G_{1,1}$	function defined by Eq. (*48*)
$G_{2,i}$	function defined by Eq. (*49*)
$G_{3,i}$	function defined by Eq. (*50*)
g	function describing the form of the amalgam surface (m)
H_i	function defined by Eq. (*52*)
h_A	height of amalgam meniscus (m)
h_i	grid interval along ξ axis
I_R	total current flowing through the decomposer model (A)
J_R	dimensionless current defined by Eq. (*31*)
j	current density (A/m^2)
j_K	cathodic current density
j_0	formal exchange current density (A/m^2)
K_j	function defined by Eq. (*53*)
k_j	grid interval along η axis
l	length of current line (m)

l_a thickness of decomposer model (m)
m, n numbers of grid points along ξ, η axes
N normal line (m)
q_h quotient of geometric series
R gas constant (8·314 J K^{-1} mol^{-1})
$R_{i,j}$ residuum
s_i distance of two neighbouring grid points
T absolute temperature (K)
t time of calculation (s)
X, Y dimensionless coordinates
X_K, Y_K dimensionless width and height of decomposer model
x, y, z coordinates (m)
x_K, y_K width and height of decomposer model (m)
Z_K parameter defined by Eq. (*26*)
Z_R dimensionless voltage defined by Eq. (*29*)
α_K cathodic charge transfer coefficient
η transformed Y coordinate
η_A, η_K anodic and cathodic overvoltage (V)
ξ transformed X coordinate
ϱ resistivity (Ω m)
τ order number of iteration
φ electric potential (V)
ψ empirical coefficient in Eq. (*57*)
$\omega_{i,j}$ overrelaxation factor defined by Eq. (*59*)
ω_0 empirical constant in Eq. (*59*)

Subscripts

A anode, am amalgam, C graphite, K cathode, i, j refer to ξ and η coordinates, M mixture of gas and electrolyte, s electrolyte side of the interface. Primes denote differentiation with respect to ξ.

REFERENCES

1. Hostomský J., Roušar I., Cezner V.: This Journal *42*, 1433 (1977).
2. Cezner V.: *Thesis*. Department of Inorganic Technology, Prague Institute of Chemical Technology, Prague (1978).
3. Regner A.: *Technická elektrochemie* I, p. 196. Academia, Prague 1967.
4. Carnahan B., Luther H. A., Wilkes J. O.: *Applied Numerical Methods*, p. 508. Wiley, New York 1969.
5. Novák P., Roušar I., Kimla A., Cezner V., Mejta V.: This Journal *45*, 1867 (1980).

Translated by K. Micka.